Research Article

Brain functional remodeling caused by sciatic nerve transposition repair in rats identified by multiple-model resting-state blood oxygenation level-dependent functional magnetic resonance imaging analysis

https://doi.org/10.4103/1673-5374.317991
Date of submission: October 27, 2020
Date of decision: December 24, 2020
Date of acceptance: April 16, 2021
Date of web publication: July 8, 2021

Yu-Song Yuan[1, 2, 3, #], Hai-Lin Xu[1, 3, #], Zhong-Di Liu[3], Yu-Hui Kou[1, 2, 3], Bo Jin[1, 2, 3], Pei-Xun Zhang[1, 2, 3, *]

Graphical Abstract *The rs-fMRI data of the rats with the proximal end of the left sciatic nerve and the distal end of the right sciatic nerve are connected through a nerve conduit*

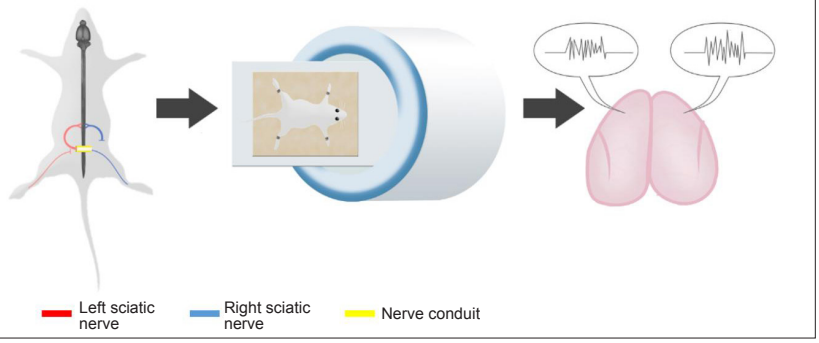

Abstract

Lower extremity nerve transposition repair has become an important treatment strategy for peripheral nerve injury; however, brain changes caused by this surgical procedure remain unclear. In this study, the distal stump of the right sciatic nerve in a rat model of sciatic nerve injury was connected to the proximal end of the left sciatic nerve using a chitin conduit. Neuroelectrophysiological test showed that the right lower limb displayed nerve conduction, and the structure of myelinated nerve fibers recovered greatly. Muscle wet weight of the anterior tibialis and gastrocnemius recovered as well. Multiple-model resting-state blood oxygenation level-dependent functional magnetic resonance imaging analysis revealed functional remodeling in multiple brain regions and the re-establishment of motor and sensory functions through a new reflex arc. These findings suggest that sciatic nerve transposition repair induces brain functional remodeling. The study was approved by the Ethics Committee of Peking University People's Hospital on December 9, 2015 (approval No. 2015-50).

Key Words: brain connectivity; brain network; fALFF; MRI; nerve transposition repair; peripheral nerve injury; ReHo; remodeling

Chinese Library Classification No. R445; R745; R456

Introduction

Trauma-induced peripheral nerve injury is common, and has a generally poor prognosis. Peripheral nerve injury is found in 1.46–2.8% of traumatic injuries, and the incidence is increasing year by year (Li et al., 2020b). In addition to the severe loss of motor and sensory functions of the affected limbs, peripheral nerve injury can also be accompanied by afferent pain, significantly impacting physical, psychological and cognitive functions, as well as overall mental health (Yang et al., 2015a, b). There are different forms of nerve or neuronal injury, including long-segment nerve defect, nerve root avulsion injury, and central hemiplegia, which usually lead to functional loss of the limbs and are the most difficult to treat. Traditional treatment methods are ineffective, especially for central lesions, and even nerve transplantation does not effectively restore the function of the target organ. Nerve transposition repair is an ideal treatment option; choosing a suitable donor for nerve translocation to repair and innervate limbs may not only help form a functional reflex arc with the center, but also reduces complications (Kotani et al., 1971;

[1]Department of Trauma and Orthopedics, Peking University People's Hospital, Peking University, Beijing, China; [2]Key Laboratory of Trauma and Neural Regeneration (Peking University), Ministry of Education, Beijing, China; [3]National Center for Trauma Medicine, Beijing, China
*Correspondence to: Pei-Xun Zhang, PhD, zhangpeixun@bjmu.edu.cn.
https://orcid.org/0000-0001-7200-2281 (Pei-Xun Zhang)
#Both authors contributed equally to this paper.

Funding: This study was supported by the National Natural Science Foundation of China, Nos. 31771322, 81671215 (to PXZ); the Beijing National Science Foundation, Nos. 7212121 (to PXZ); the National Key Research and Development Plan of China, No. 2018YFB1105504 (to PXZ); Shenzhen Science and Technology Plan Project, No. JCYJ20190806162205278 (to PXZ); Sanming Project, No. SZSM202011001 (to PXZ); the Fundamental Research Funds for the Central Universities, Clinical Medicine Plus X - Young Scholars Project of Peking University China, No. PKU2020LCXQ020 (to YHK); the Key Laboratory of Trauma and Neural Regeneration (Peking University), the Ministry of Education China, No. BMU2019XY007-01; and the Ministry of Education Innovation Program of China, No. IRT_16R01.
How to cite this article: Yuan YS, Xu HL, Liu ZD, Kou YH, Jin B, Zhang PX (2022) Brain functional remodeling caused by sciatic nerve transposition repair in rats identified by multiple-model resting-state blood oxygenation level-dependent functional magnetic resonance imaging analysis. Neural Regen Res 17(2):418-426.

Kawabata et al., 2001; Lam Van Ba et al., 2018; Zheng et al., 2018; Li et al., 2020a). However, even with an appropriate nerve repair method, the recovery of nerve function, to date, is not ideal. There is a therapeutic limit to repairing the nerve from the periphery determined by the tissue characteristics of the nerve itself. Treating a nerve injury through a central approach can improve the prognosis of peripheral nerve injury.

Brain neuroplasticity has been extensively studied in recent years. The brain can regain lost functions caused by injury through learning and training. Brain neuroplasticity can be divided into structural plasticity and functional plasticity (Dąbrowski et al., 2019; Chen et al., 2020). In structural plasticity, synapses and neurons establish new connections during learning and experience, thereby affecting behavior. In functional plasticity, a function controlled by an affected brain area can be taken over by an adjacent area through learning and training, and the injured region can regain some function through learning and training as well (Zhang and Chopp, 2009).

In recent years, resting-state blood oxygenation level-dependent functional magnetic resonance imaging (rs-fMRI) has become a promising method in brain science (Barkhof et al., 2014). Rs-fMRI is a non-invasive imaging method that can avoid task interference (Chao-Gan and Yu-Feng, 2010). To clearly obtain visual information on brain functional areas post central remodeling induced by translocation repair, we designed a model of lower extremity nerve translocation repair. Herein, we investigated the features of functional remodeling of brain functional areas following sciatic nerve injury repair by nerve transposition in the lower limbs, with the aim of providing insight for future investigations and clinical treatments. To the best of our knowledge, this study is the first to describe brain remodeling processes following lower limb nerve transposition repair in rats.

Materials and Methods

Animals

Because male rats would become very large by the end of the study duration of nearly 1 year, which would make it difficult to carry out experimental procedures, only female rats were included in this study. A total of 36 specific-pathogen-free grade 6-week-old female Sprague-Dawley rats (weighing 200–220 g) were obtained from Beijing Weitong Lihua Experimental Animal Co., Ltd. (license No. SCXK (Jing) 2016-0006). The generation of the animal model and breeding were carried out in the Animal Center of Peking University People's Hospital under a 12-hour light/dark cycle, and 40% humidity. All experimental and feeding procedures were approved by the Ethics Committee of Peking University People's Hospital on December 9, 2015 (approval No. 2015-50). Experimental animal suffering was minimized in all experimental procedures to the best of our ability.

Groups and surgery

A total of 36 rats were randomly divided into the following two groups: the sciatic nerve transposition repair group (surgery group, n = 21) and the normal control group (control group, n = 15). In the surgery group, the right hind limb was termed the cross group, while the left hind limb was termed the denervation group during analysis.

Rats in the surgery group were placed in a prone position following isoflurane (Shenzhen Reward Life Technology Co., Ltd., Shenzhen, China) anesthesia (5% induction anesthesia, 5% maintenance anesthesia, 100 mL/min). The lower limbs and the rear half of the back were shaved. The skin was cut along the long axis of the left femur after disinfecting to expose the sciatic nerve. The sciatic nerve was freed and cut at the bifurcation. The distal stump of the left sciatic nerve was ligated after the left sciatic nerve was cut off. After covering the left sciatic nerve with muscle, the right sciatic nerve was exposed, disconnected at the deep surface of the piriformis muscle, and the proximal stump of the sciatic nerve was ligated. The back skin was cut along the line of the upper iliac crests. A 4-mm chitin conduit (Peking University People's Hospital and Chinese Textile Academy, Patent No. 01136314.2) was used to cover the proximal end of the left sciatic nerve and the distal end of the right sciatic nerve with 10-0 suture, with a gap of about 2 mm between the nerve ends. The fascia and skin were sequentially sutured. Rats were placed in a new rat cage after the blood stains on the skin were wiped off. The control group received no treatment.

Neuroelectrophysiological testing

Six rats in each of the experimental and control groups were tested at 8 months after the operation. The skin was cut along the axial line of the right hind limb to expose the tibialis anterior and gastrocnemius muscles after isoflurane anesthesia (5% induction anesthesia, 5% maintenance anesthesia, 100 mL/min). The sciatic nerve and its branches were bluntly separated. Stimulation electrodes were placed at two locations in the common peroneal nerve, at 10 mm apart, and induction electrodes were placed on the tibialis anterior muscle. The stimulation parameters on the electrophysiological device (Synergy Electrophysiology Instrument, Oxford, UK) were 0.09 mA current intensity and 0.1 ms duration. The Δt between the two incubation periods and length (L) of the neural stem between the two stimulation points were calculated. The motor nerve conductive velocity (MNCV) was measured in L/t, with t representing the time between the two stimulations. The MNCV of the tibial nerve was measured by the same method.

Osmium acid staining

Eight months post-surgery, the transpositioned repaired nerves (n = 6 rats/group) were exposed along the surgical incision after nerve electrophysiological testing was completed. Then, 3-mm nerve sections at the proximal and distal ends of the conduit were harvested, fixed with 4% paraformaldehyde, and stained with 1% osmium acid (Beijing Chemical Factory Co., Ltd., Beijing, China) for 12 hours. After rinsing for 6 hours under running water, a graded ethanol series was used for dehydration, and xylene was used for clearing. Samples were embedded in paraffin, sliced into 1-μm sections, and sealed with neutral resin after dewaxing. The sections were observed under the light microscope (Olympus Corporation, Tokyo, Japan) and imaged.

Wet muscle weight

The anterior tibialis and gastrocnemius tendon were severed from the ankle joint, peeled away from the far and near ends, and cut off at the proximal ends after electrophysiological testing was completed. The muscles were weighed on an electronic balance (FA2004, Shanghai Shunyu Hengping Scientific Instrument Co., Ltd., Shanghai, China) immediately after wiping the muscle surface with gauze.

Hematoxylin-eosin staining of muscle tissue

The central part of the anterior tibialis was hematoxylin-eosin-stained after measuring the wet weight. Muscles were fixed with 4% paraformaldehyde and stored at 4°C overnight. A graded ethanol series was used for dehydration, and xylene was used for clearing. Samples were embedded in paraffin and sliced into 5-μm sections. Sections were used for conventional hematoxylin-eosin staining and sealed with neutral resin after dewaxing. The slices were observed under the light microscope and imaged.

Magnetic resonance imaging data acquisition

At 12 months post-surgery, fMRI data acquisition was carried out on a 7.0T small animal magnetic resonance imager

(PharmaScan 70/16 US, Bruker, Switzerland). Rats (n = 9 in the surgery group and 5 in the control group) were anesthetized with isoflurane gas (5% induction anesthesia, 5% maintenance anesthesia, 100 mL/min). The following scan sequences and parameters were used to obtain axial imaging information of the rat brain.

T2-weighted imaging: the scanning sequence was T2_TurboRare. Specific parameters: repetition time/echo time = 5600/33 ms; image size: 256 × 256; field of view: 35 mm × 35 mm; slice thickness: 0.55 mm; slices: 50; averages: 2; scan time: 5 minutes, 58 seconds.

Rs-fMRI: The scanning sequence was T2star_FID_EPI. Specific parameters: repetition time/echo time = 2.000/20 ms; image size: 64 × 64; Field of view: 35 mm × 35 mm; slice thickness: 0.55 mm; slices: 50; averages: 1; repetition: 600; scan time: 20 minutes.

Fractional amplitude of low frequency fluctuations and regional homogeneity data analysis

Data pre-processing was performed with the spmratIHEP toolbox using statistical parametric mapping (SPM8; https://www.fil.ion.ucl.ac.uk/spm/software/spm8/) and resting-state fMRI Data Analysis Toolkit (REST) software (http://www.restfmri.net/forum). The regional homogeneity (ReHo) and fractional amplitude of low frequency fluctuations (fALFF) measurements were analyzed and compared between the control and surgery groups using spmratIHEP with SPM8 and REST software which, as described by Nie et al. (2010, 2013, 2014).

A linear model was used to remove any observed trends in the normalized images. To reduce the effects of low-frequency and high-frequency drift, the images were temporally band-pass-filtered. Kendall's coefficient was calculated to assess the ReHo value (Nie et al., 2010, 2013, 2014).

Rs-fMRI data analysis

All functional image post-processing and data analysis were done with the spmratIHEP toolbox in SPM8 software, consisting of an fMRI rat standard brain template and atlas in Paxinos & Watson space (Liang et al., 2017), as previously described (Nie et al., 2010, 2013, 2014). Seed-based correlational analyses on a voxel-by-voxel basis were used to evaluate brain functional connectivity with spmratIHEP. The time course attributes were calculated and used to quantify the strength of the functional connectivity to establish a functional connectivity map.

Statistical analysis

All data are expressed as mean ± standard deviation (SD). The results of related data of neurological function testing were statistically analyzed with SPSS 17.0 software (SPSS, Chicago, IL, USA). An independent samples t-test was performed to assess differences in MNCV, fALFF and ReHo values. The cerebral regions with significant differences in fALFF and ReHo values between the two groups were selected, with a voxel-level height threshold of $P < 0.005$ and a cluster-extent threshold of 20 voxels. Cronbach's α of the MNCV was 0.05.

One-way analysis of variance was used to assess differences in muscle weight that conformed with normality and homoscedasticity. Least significant difference test was used for further pairwise analysis. Non-parametric test (Kruskal–Wallis k samples) was conducted if the data did not conform with normality or homoscedasticity. Cronbach's α was set at 0.05.

Graph metrics between the surgery and control groups were compared with two-sample t-test. For global metrics, we compared the metrics at all thresholds. For nodal metrics, we compared the area under the curve first, and then compared the metrics at all thresholds. We also compared the differences in functional connectivity between the surgery and control groups using network-based analysis in MATLAB (https://www.mathworks.com) and BrainNet Viewer (https://www.nitrc.org/projects/bnv). Cronbach's α was 0.05.

Results

General observation of sciatic nerve transposition repair in rats

A total of five rats in the surgery group and four rats in the control group died prior to final testing. A brain tumor was detected by MRI in one of the rats in the surgery group, and was accordingly excluded. Six rats in each group received electrophysiological testing and histological staining at 8 months after surgery. Nine rats in the surgery group and five rats in the control group were tested by fMRI, 12 months after surgery.

At 8 months post-surgery, the nerve suture area was covered with connective tissue with no neuroma or neuroedema. The conduits were partially absorbed. In the denervation group, the foot ulcer was found to be swollen, and normal foot anatomy could not be distinguished. The cross group showed obvious signs of atrophy and some autophagy (**Figures 1** and **2**).

Motor nerve conduction velocity in rats with sciatic nerve transposition repair

When the right common peroneal nerve and tibial nerve were stimulated in the surgery group, dorsiflexion and plantar flexion of the right hind limb was observed. The conduction velocities of the common peroneal and tibial nerves in the cross group were lower compared with the control group ($P < 0.05$; **Table 1**).

Regeneration of the sutured nerve in rats with sciatic nerve transposition repair

Osmium acid staining showed that compared with the control group, the myelin sheath of myelinated nerve fibers in the cross group was thinner, sparsely distributed, and lighter in color. The nerves in the cross group were regenerated to an extent, and many myelinated nerve fibers were visible (**Figure 3**).

Muscle wet weight in rats with sciatic nerve transposition repair

The cross and denervation groups had obvious signs of atrophy of the anterior tibialis and gastrocnemius. The anterior tibialis and gastrocnemius in the denervation group resembled a tendon, and the anterior tibialis and gastrocnemius muscles in the cross group were also indistinguishable in terms of

Table 1 | **Results of neuro-electrophysiological tests and muscle wet weights in rats with sciatic nerve transposition repair at 8 months post-surgery**

Group	PN MNCV (m/s)	TN MNCV (m/s)	Gastrocnemius (g)	Anterior tibialis (g)
Control (n = 5)	66.28±1.15	77.32±3.67	1.85±0.06$^{\#}$	0.62±0.07$^{\#}$
Denervation (n = 9)	NA	NA	0.10±0.01*	0.11±0.02*
Cross (n = 9)	40.50±1.78*	42.36±1.37*	0.75±0.06$^{*\#}$	0.42±0.03$^{*\#}$

All data are expressed as mean ± SD, and were analyzed by independent samples t-test (MNCV) or one-way analysis of variance followed by the least significant difference test (muscle weight). *$P < 0.05$, vs. control group; #$P < 0.05$, vs. denervation group. MNCV: motor nerve conduction velocity; NA: not applicable; PN: common peroneal nerve; TN: tibial nerve.

their muscle tendon, tendon-abdominal joint, and abdominal muscle content. The wet weights of the anterior tibialis and gastrocnemius were significantly lower in the cross group compared with the control group ($P < 0.05$), but significantly greater compared with the denervation group ($P < 0.05$; **Table 1**).

Muscle fibers in the central part of the anterior tibialis in rats given sciatic nerve transposition repair

The muscle fibers in the control group were tightly arranged, with sharp edges and corners, and no pathological features were observed. The gaps between the muscle fibers in the cross group were increased and the diameter of the muscle fibers was smaller compared with the control group. Circular muscle fibers were seen, with less infiltration of connective tissue. In the denervation group, muscle fibers were filled with fat and connective tissue, and they showed signs of obvious atrophy (**Figure 4**).

Magnetic resonance imaging in different brain regions in rats given sciatic nerve transposition repair

fALFF value

The fALFF values of eight brain regions in the left hemisphere and 13 brain regions in the right hemisphere were significantly higher in the surgery group compared with the control group ($P < 0.005$; **Table 2** and **Figure 5**). The fALFF values of 10 brain regions in the left hemisphere and 6 brain regions in the right hemisphere were lower in the surgery group compared with the control group ($P < 0.005$; **Table 2** and **Figure 5**).

ReHo value

The ReHo values of eight brain regions in the left hemisphere and 11 brain regions in the right hemisphere were significantly higher in the surgery group compared with the control group ($P < 0.005$; **Table 3** and **Figure 6**). The ReHo values of 16 brain regions in the left hemisphere and 19 brain regions in the right hemisphere were lower in the surgery group compared with the control group ($P < 0.005$; **Table 3** and **Figure 6**).

Global metrics in different brain regions in rats with sciatic nerve transposition repair

A significantly different normalized characteristic path length (lambda) was found between the surgery and control groups at low range thresholds ($P < 0.05$). There was no significant difference in other indicators (**Figure 7**).

Table 2 | Fractional amplitude of low frequency fluctuation values in different brain regions in rats with sciatic nerve transposition repair at 8 months post-surgery

			Montreal Neurological Institute Coordinates		
Region	**Hemisphere**	**Max_T**	***X***	***Y***	***Z***
Surgery group > control group					
Dentate gyrus	Left	4.0078	–2.75	3.4372	–5.158
Hippocampus	Left	3.9634	–1.94	2.5779	–4.918
Insular cortex	Left	3.7013	–6.3	6.5554	0.1221
Midbrain periaqueductal gray matter	Left	3.9588	–0.6	5.6393	–5.638
Midbrain superior colliculus	Left	4.6283	–2.47	3.779	–5.638
Midbrain tegmentum of midbrain	Left	4.5716	–0.88	5.8816	–5.158
Pt pretectal area	Left	5.1933	–2.47	3.7364	–5.158
Thalamus lateral nucleus group	Left	5.7444	–2.75	4.0213	–5.158
Dentate gyrus	Right	3.1065	2.881	3.8261	–5.878
Hippocampus	Right	3.9101	2.614	3.5731	–6.598
Insular cortex	Right	3.1406	2.614	3.874	–6.598
Midbrain inferior colliculus	Right	3.9022	2.63	3.9805	–7.798
Midbrain superior colliculus	Right	3.7519	2.354	3.5581	–6.598
Nucleus ccumbens	Right	3.4274	1.706	6.6084	1.5621
Olfactory cortex	Right	3.8294	3.7	7.5258	–7.558
Pontine basilar part of pons	Right	3.2318	3.706	7.8516	–8.038
Pontine tegmentum of pons	Right	3.1309	3.447	7.2525	–8.038
Retrosplenial cortex	Right	3.4198	1.811	2.9004	–6.118
Sensory cortex	Right	3.4476	5.439	2.1303	1.8021
Striatum	Right	4.7854	3.871	6.2761	0.1221
Thalamus lateral nucleus group	Right	3.8114	2.627	3.6583	–7.558
Surgery group < control group					
Aanterior lobe of cerebellum	Left	5.4965	–4.024	3.7436	–9.4779
Frontal association cortex	Left	3.5961	–1.554	1.9513	5.8821
Hippocampus	Left	5.5734	–4.031	3.4001	–8.9979
Olfactory bulb	Left	4.0005	–1.561	1.3246	6.3621
Olfactory cortex	Left	3.6063	–5.11	3.0123	–8.5179
Poaterior lobe of cerebellum	Left	7.6226	–4.024	3.1595	–9.4779
Retrosplenial cortex	Left	7.8249	–4.031	2.816	–8.9979
Temporal association cortex	Left	6.0339	–5.37	2.4132	–8.5179
Visual cortex	Left	4.752	–5.376	2.0697	–8.0379
Anterior lobe of cerebellum	Right	3.8287	2.6732	3.9565	–10.918
Olfactory bulb	Right	3.8047	0.8407	2.0264	6.6021
Olfactory cortex	Right	5.2012	4.7887	4.1897	–8.7579
Olfactory tract	Right	3.3828	1.0903	2.5616	7.3221
Poaterior lobe of cerebellum	Right	3.822	2.6732	2.7883	–10.918
Visual cortex	Right	3.9557	3.4599	0.9126	–8.9979

$P < 0.005$; cluster size = 20 voxels.

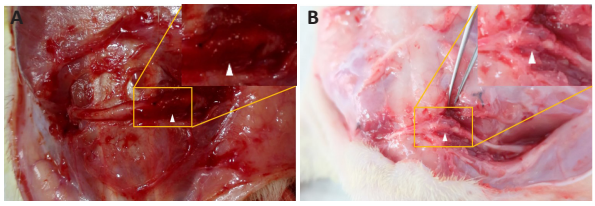

Figure 1 | Observation of the surgical zone in rats given sciatic nerve transposition repair.
(A) Surgical zone just post-surgery. (B) Surgical zone at 8 months post-surgery. The sutured nerve under the skin. The white triangles mark the conduit.

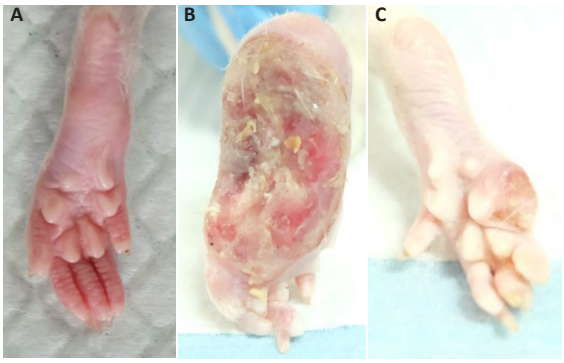

Figure 2 | Observation of the hind limbs in rats with sciatic nerve transposition repair.
(A) Full muscle and normal skin of a normal foot. (B) The foot is swollen, ulcerated, and bones are visible in the denervation group. (C) The foot muscles are atrophied, and the skin is ruptured in the cross group.

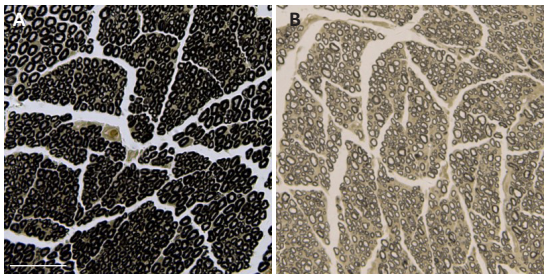

Figure 3 | Morphology of myelinated nerve fiber sheaths in rats with sciatic nerve transposition repair at 8 months post-surgery (osmium acid staining).
(A) The myelin sheath of the control group was darker. Myelinated nerve fibers were densely arranged. (B) The myelin sheaths of the cross group were light. Myelinated nerve fibers were sparsely arranged. Black circles represent the sheaths of myelinated nerve fibers. Scale bar: 50 μm.

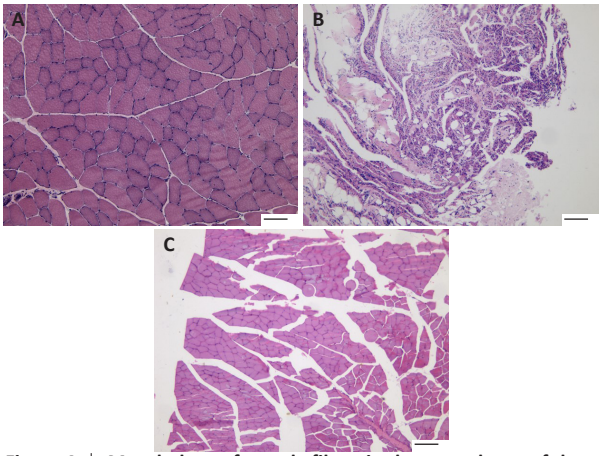

Figure 4 | Morphology of muscle fibers in the central part of the anterior tibialis of rats given sciatic nerve transposition repair at 8 months post-surgery (hematoxylin-eosin staining).
(A) The muscle fibers in the control group were round and full, and were tightly arranged. (B) The muscle fibers in the denervation group showed significant atrophy, with a large amount of connective tissue between the muscle fibers. (C) The muscle fibers in the cross group were slightly atrophic. Scale bars: 100 μm.

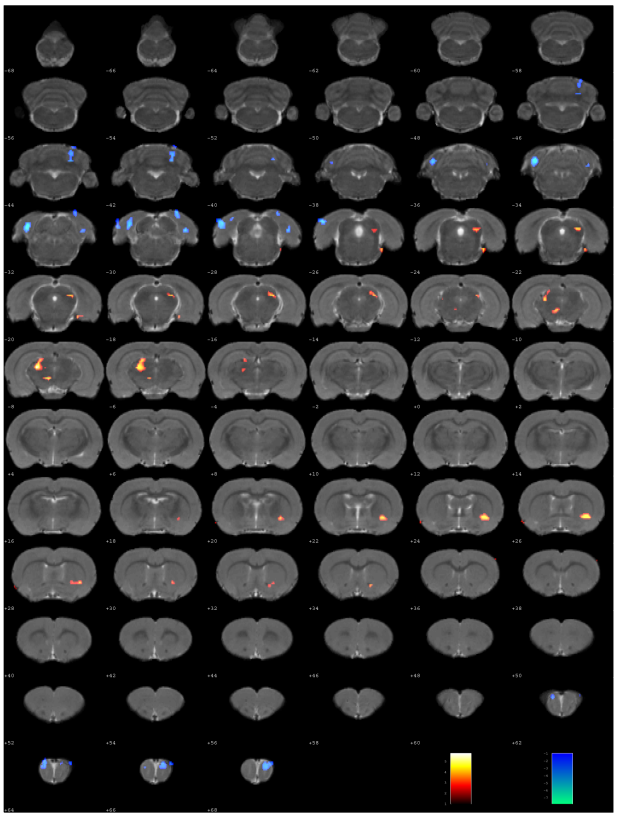

Figure 5 | Resting-state fALFF maps of the whole brain compared between sciatic nerve transposition repair and normal rats at 8 months post-surgery.
Each column represents coronal slices. The color bar reflects mean values. The red and blue respectively represent increased and decreased fALFF signals relative to the control group. fALFF: Fractional amplitude of low frequency fluctuations.

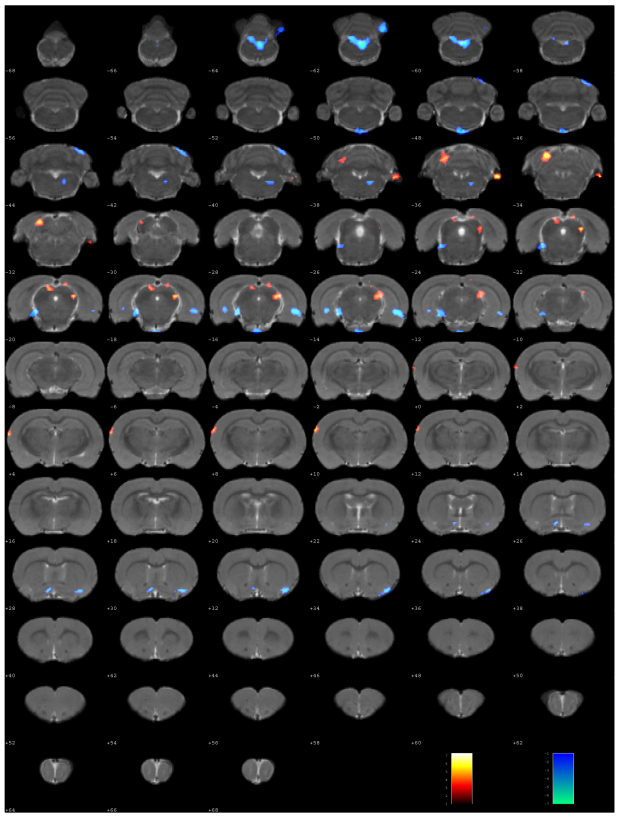

Figure 6 | Resting-state ReHo maps of the whole brain compared between sciatic nerve transposition repair and normal rats at 8 months post-surgery.
Each column represents coronal slices. The color bar reflects mean values. The red and blue respectively represent increased and decreased ReHo signals relative to the control group. ReHo: Regional homogeneity.

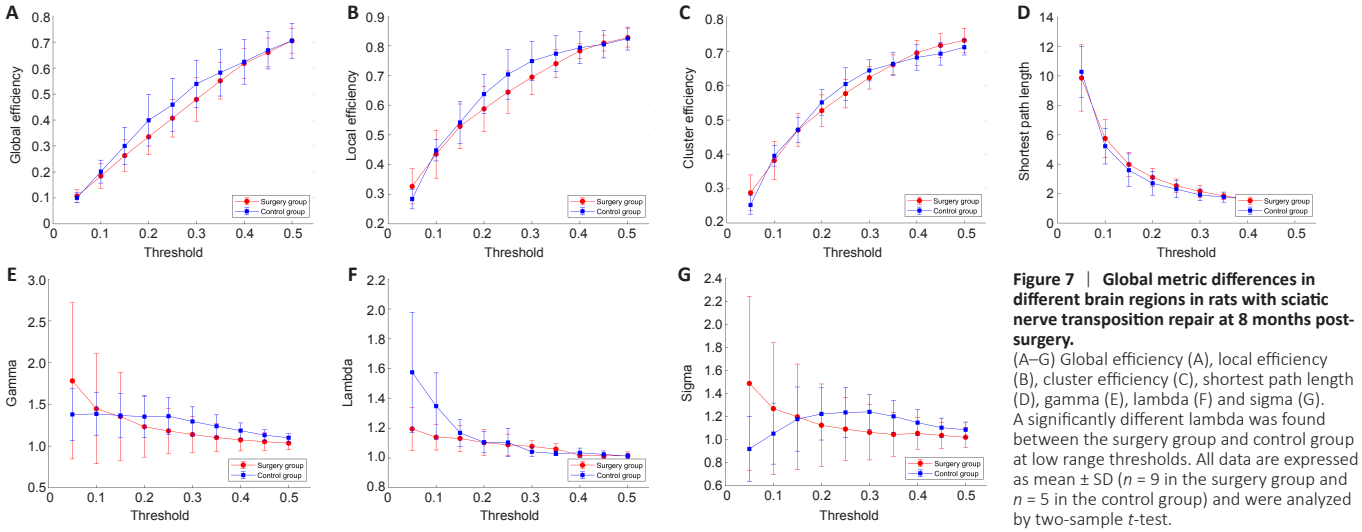

Figure 7 | Global metric differences in different brain regions in rats with sciatic nerve transposition repair at 8 months post-surgery.
(A–G) Global efficiency (A), local efficiency (B), cluster efficiency (C), shortest path length (D), gamma (E), lambda (F) and sigma (G). A significantly different lambda was found between the surgery group and control group at low range thresholds. All data are expressed as mean ± SD (n = 9 in the surgery group and n = 5 in the control group) and were analyzed by two-sample t-test.

Local metrics in different brain regions in rats with sciatic nerve transposition repair

The right olfactory bulb, right thalamus and right temporal association areas showed significant differences between the control and surgery groups (P < 0.05). However, only the right temporal association cortex showed significant differences at a low threshold (P < 0.05; **Figure 8**).

Rich-club in different brain regions of rats with sciatic nerve transposition repair

There was no difference in rich-club, feeder or local strength between the control and surgery groups (P > 0.05; **Figure 9**).

Discussion

The human brain network is extremely complex and efficient, and is formed by multiple brain regions responsible for different functions based on the principles of compartmentalization and integration. This system enables internal functional coordination, monitoring, and feedback from the surroundings. The functional characteristics of the brain's structural organization reveal the coordination of different functional brain regions. This requires efficient coordination in functional partitioning and functional integration to form a brain topological network, i.e. brain connectivity (Gorrostieta et al., 2012). Numerous studies have demonstrated that the loss of motor and sensory functions leads to disturbances in functional connections involving the sensorimotor cortex. As sensory-motor network activities change, some advanced functional networks, such as the default mode network, dorsal attention network, salience network, executive control network, and other cognitive association networks, may undergo direct or indirect changes

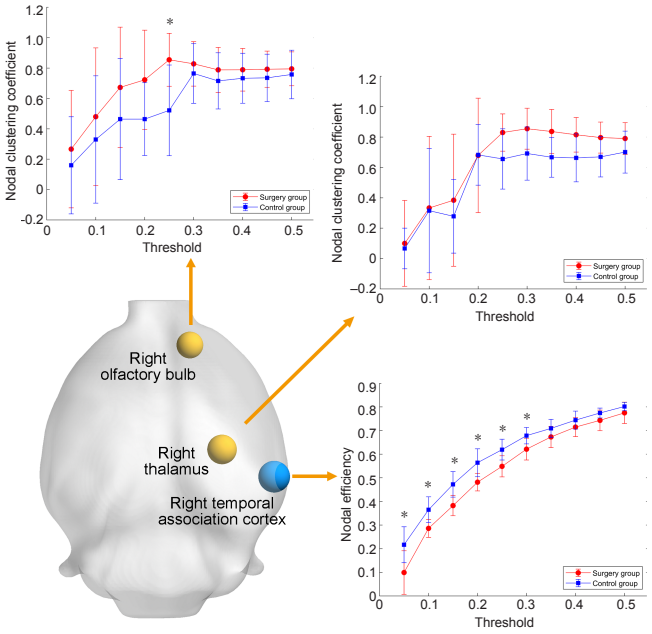

Figure 8 | Local metric differences in different brain regions in rats with sciatic nerve transposition repair.
Compared with the control group, the surgery group showed higher AUC of the nodal clustering coefficient in the right olfactory bulb (yellow node) and thalamus (yellow node), and lower AUC values of nodal efficiency in the right temporal association cortex (blue node). All data are expressed as mean ± SD (n = 9 in the surgery group, and n = 5 in the control group), and were analyzed by two-sample t-test. AUC: Area under the curve.

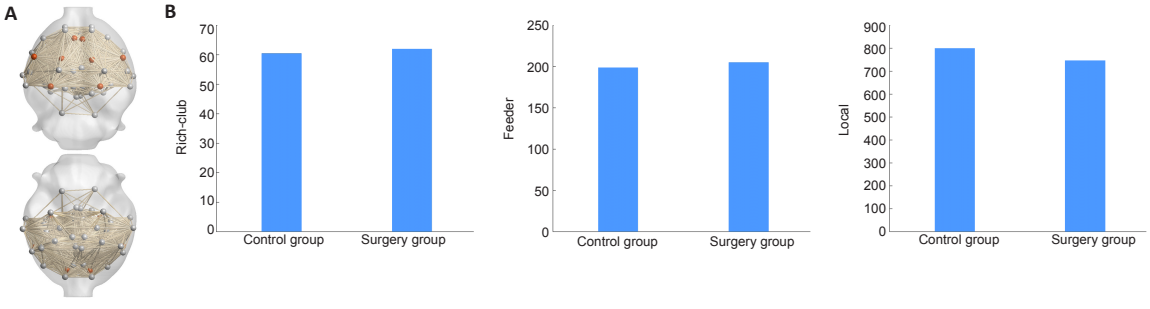

Figure 9 | Overall topological properties of the brain in rats with sciatic nerve transposition repair.
(A) Bilateral motor cortex, orbital cortex, sensory cortex and visual cortex were hubs (red nodes) (defined as having a nodal degree of at least 1 standard deviation above the mean nodal degree across all regions) of the functional network. (B) There was no significant difference in the rich-club, feeder or local strength between the surgery group (n = 9) and the control group (n = 5) (P > 0.05). Data were analyzed by two-sample t-test.

Table 3 | **Regional homogeneity values in different brain regions in rats with sciatic nerve transposition repair**

Region	Hemisphere	MAX_T	Montreal Neurological Institute coordinates		
			X	*Y*	*Z*
Surgery group > control group					
Auditory cortex	Left	4.6054	–7.3107	3.288	–3.2379
Cerebellum anterior lobe of cerebellum	Left	7.2665	–2.4155	2.3675	–9.4779
Insular cortex	Left	4.3425	–0.8602	2.2252	–6.8379
Midbrain inferior colliculus	Left	4.5611	–2.4221	2.3249	–8.9979
Midbrain superior colliculus	Left	4.3155	–0.8569	2.2465	–7.0779
Retrosplenial cortex	Left	4.389	–1.1164	1.9483	–7.0779
Sensory cortex	Left	5.035	–7.3173	2.9622	–2.7579
Corpus callosum	Right	3.508	1.818	1.7748	–6.5979
Dentate gyrus	Right	3.5521	2.8807	3.8261	–5.8779
Flocculonodular lobe	Right	7.0706	5.5977	6.6573	–9.7179
Hippocampus	Right	4.9564	2.8939	3.9113	–6.8379
Insular cortex	Right	4.4977	2.6138	3.874	–6.5979
Midbrain inferior colliculus	Right	4.8041	2.9071	3.9965	–7.7979
Midbrain superior colliculus	Right	4.0694	2.6171	3.8953	–6.8379
Olfactory cortex	Right	3.834	5.5878	6.2925	–8.9979
Retrosplenial cortex	Right	3.964	1.8312	1.5768	–7.5579
Thalamus lateral nucleus group	Right	5.3878	2.9038	3.9752	–7.5579
Visual cortex	Right	3.2309	1.5313	0.8276	–5.8779
Surgery group < control group					
Accumbens nucleus	Left	3.2652	–0.9691	6.7792	1.0821
Basilar part of pons	Left	4.6385	–0.3272	9.545	–6.5979
Bed nucleus of stria terminalis	Left	3.3486	–1.2121	7.1716	–0.1179
Dentate gyrus	Left	4.0171	–5.1432	5.7198	–6.1179
Hippocampus	Left	3.9521	–3.5244	6.4608	–6.8379
Hypothalamus_preoptic region	Left	4.1003	–1.2154	7.1503	0.1221
Medulla oblongata	Left	4.8437	0.0486	7.2795	–13.7979
Olfactory cortex	Left	3.4662	–3.5145	6.5247	–7.5579
Poaterior lobe of cerebellum	Left	5.0251	–1.0174	6.3751	–14.2779
Ptpretectal area	Left	3.2488	–2.7418	6.1207	–5.8779
Septal area	Left	3.6481	–0.689	6.8165	0.8421
Striatum	Left	4.5272	–1.222	7.1077	0.6021
Tegmentum of midbrain	Left	3.9067	–2.9782	6.2548	–7.5579
Tegmentum of pons	Left	4.6226	–3.2616	6.1962	–7.0779
Thalamus_lateral nucleus group	Left	4.2983	–3.2616	5.913	–7.0779
Thalamus_medial nucleus group	Left	5.1254	0.0552	7.0212	–14.2779
Accumbens nucleus	Right	3.0662	2.7883	7.6016	0.8421
Amygdaloid body_right	Right	3.8378	0.0222	10.0296	–11.8779
Anterior commissure	Right	4.2099	0.0486	6.6954	–13.7979
Basilar part of pons	Right	4.5343	–0.0504	9.561	–6.5979
Cerebellar nucleus	Right	3.4858	3.5259	5.1441	–13.7979
Corpus callosum	Right	5.4826	5.8316	6.6796	–6.5979
Dentate gyrus	Right	3.5026	5.2887	6.606	–6.1179
Hippocampus	Right	5.8376	6.0845	6.652	–6.1179
Insular cortex	Right	3.3252	4.6534	7.1042	1.0821
Medulla oblongata	Right	7.0274	0.5849	7.0096	–13.7979
Olfactory cortex	Right	5.5562	6.0911	6.6946	–6.5979
Olfactory tubercle	Right	3.3254	3.0346	7.8323	1.8021
Piriform cortex	Right	4.2667	3.8609	7.3804	0.8421
Poaterior lobe of cerebellum	Right	3.7767	3.2161	1.9946	–11.3979
Septal area	Right	5.2281	0.0486	6.9786	–13.7979
Striatum	Right	4.1367	3.5841	7.3644	0.8421
Tegmentum of midbrain	Right	4.5186	0.0189	10.2915	–11.6379
Tegmentum of pons	Right	3.6476	1.5841	7.5935	–9.7179
Thalamus_medial nucleus group	Right	3.7575	0.0453	6.9573	–13.5579

$P < 0.005$; cluster size = 20 voxels.

(Gao and Lin, 2012). These changes are not only limited to movement and sensory-related cortical connections, but also occur at a higher cognitive level (Auer et al., 2009; Makin et al., 2015; Feng et al., 2016; Bhat et al., 2017).

Nerve repair therapy takes advantage of the brain's intrinsic plasticity through neuronal remodeling, neurogenesis, and axonal regeneration (Ciumas et al., 2008). During motor learning, changes in temporal accuracy and flexibility involve

multiple overlapping processes (Diedrichsen and Kornysheva, 2015). Learning recruits new neurons that were not previously involved in the learning process (Costa et al., 2004). Bhat et al. (2017) found that compared with the control group, the functional connection of the anterior cingulate gyrus, right upper frontal gyrus, and left insular cortex in patients with unilateral brachial plexus ganglion injury was reduced. In patients with improved muscle strength following surgery, the functional connections of the left auxiliary motor cortex, medial frontal gyrus, and anterior cingulate cortex were enhanced (Bhat et al., 2017). Lu et al. (2016) found that compared with the normal control group, the functional connectivity of the supplementary motor area and multiple brain areas, including the anterior wedge, posterior cingulate gyrus and anterior cingulate gyrus, were decreased in patients with unilateral brachial plexus injuries. However, their findings remain controversial. Liu et al. (2013) found no difference in functional connectivity between patients with unilateral brachial plexus injury and a healthy control group, while Feng et al. (2016) found that the functional connectivity between the default mode network and executive control network in patients with unilateral total brachial plexus injury was greater than that in healthy controls.

Nerve transposition repair technologies are increasingly valued and considered an important treatment method for certain types of nerve injury (Yu et al., 2019; Xie et al., 2020). This repair technique constructs a new nerve reflex arc. Based on the method of contralateral brachial plexus nerve repair using the healthy C7 nerve root (Zheng et al., 2018), the left sciatic nerve was translocated to repair the right sciatic nerve. The nerve was found to have regenerated, based on histological observations, at 8 months post-surgery. The electrophysiological testing results showed that the nerve conduction (transmission) function of the nerve was restored to an extent, and that it was able to control the movement of the right hind limb. Some signs of autophagy were observed in the toes of the right hind limb, while the left hind limb looked significantly better, indicating that the sensory function of the right hind limb had also been restored to a degree (Tos et al., 2009). The muscle atrophy of the right hind limb was significantly less severe than that of the denervated muscle on the left, indicating that the repaired nerve could effectively innervate and protect the target organ. The results of the nerve function tests showed that following transposition repair, the nerves could effectively handle the motor and sensory functions of the receptor area, indicating that the central nervous system had indeed been remodeled.

The ALFF analysis method first passes the time series of each voxel through a 0.01–0.08 Hz band-pass filter to retain the blood oxygenation level-dependent signal in the low frequency band. This method reflects functional connectivity by measuring the spatiotemporal correlation between spatially separated brain regions (Yang et al., 2007). The ALFF method reflects the spontaneous activity of brain neurons by directly observing the amplitude of the baseline changes of the brain's blood oxygenation level-dependent signal (Fox and Raichle, 2007). Zou et al. (2008) improved the original ALFF method, defining the low frequency band (0.01–0.08 Hz) relative to the full-frequency power spectrum as the fALFF, effectively solving the problem linked to using ALFF in physiological noise-sensitive contexts.

In this study, the fALFF values of the bilateral dentate gyrus, hippocampus, insular cortex, midbrain superior colliculus and thalamic lateral nucleus were higher in the surgery group than in the control group. This may indicate that the remodeling of these regions was caused by the responses of all brain regions involved in the default mode network and dorsal attention network. The higher fALFF values of the midbrain periaqueductal gray matter, midbrain tegmentum and pretectal area in the left hemisphere of the surgery group may be caused by the loss of target innervation. The higher fALFF values in the midbrain inferior colliculus, nucleus accumbens, olfactory cortex, basilar part of the pons, pontine tegmentum, retrosplenial cortex, sensory cortex and striatum in the right hemisphere indicate that the transposition repair not only changed the motor functions of the cortex, but also the sensory functions in this animal model.

The ReHo assumes that the time series of adjacent voxels in an active functional area are similar. The Kendall's Coefficient of Concordance is used to measure this similarity (also called the ReHo value). The ReHo value reflects the synchronization of the local blood oxygenation level-dependent signal time series in the brain area, not the signal strength (Zang et al., 2004). Compared with the control group, the ReHo values of the bilateral insular cortex, midbrain inferior colliculus, midbrain superior colliculus, hippocampus and retrosplenial cortex were higher in the surgery group. This may suggest that these regions manipulate the whole brain to adapt to the changes caused by surgery. Accordingly, the regional homogeneity of the sensory brain regions of the right hemisphere, including the thalamic lateral nucleus, olfactory cortex and flocculonodular lobe, were also enhanced.

There was no difference in fALFF or ReHo value in the motor cortex in the whole brain between the two groups, which might be caused by the resting state. Differences might be revealed in the task state.

There was no difference in whole brain connectivity between the two groups, except for the lambda values at low range thresholds, demonstrating that the information delivery efficiency decreased after remodeling. However, these changes do not imply that the functional connectivity of the entire brain had changed, which would entail that sciatic nerve transposition repair surgery does not fundamentally change the efficiency of the functional connectivity of the brain.

There are some limitations to this study. Ideally, a group should have been added to exclude the effects of nerve damage. However, the changes in the right hemisphere of rats in the surgery group can represent the results of sciatic nerve transposition repair to a degree from fMRI data. The changes in the left cerebral hemisphere could be regarded as the result of paw denervation to an extent. Therefore, we reduced the number of groups based on animal ethics considerations. We will undertake a more detailed study in the future. Brain remodeling is a very complicated process. Here, we only examined a single time point in this cross-sectional study, which therefore cannot evaluate the dynamic processes inherent in brain remodeling. However, to the best of our knowledge, this is the first study of brain remodeling following the creation of a new reflex arc across the length of the spinal cord caused by nerve transposition repair, thereby shedding light on brain remodeling caused by nerve transposition repair of the lower extremities.

In summary, the brain regions in the dorsal attention network and default mode network may be remodeled at rest following nerve transposition repair, which may incur permanent changes to neurological functions. Brain regions function through complex network systems involving the entire brain. In other words, the sensorimotor cortex is not independent, and the remodeling of sensorimotor regions may cause a series of changes in other regions of the brain responsible for other complex functions, as similarly concluded by Markov et al. (Markov et al., 2013). The metabolic and other changes in the corpus callosum of the hemisphere that had lost the target organ could enhance the efficiency of information transfer between the two hemispheres. The regional homogeneity of the motor cortex and vision-related brain regions corresponding to the repaired limb were enhanced following nerve repair. Sciatic nerve transposition repair did

not change the brain's functional connectivity network nor its efficiency at a resting state, potentially due to the inactive neurons in the resting state.

The sciatic nerve transposition created a new reflex arc to make it possible for the brain functional zone to control a new target organ based, at least to a degree, on the functional remodeling of brain networks during the resting state. Functional remodeling in the task state and the structural changes in the brain will be investigated by diffusion tensor imaging in a future study, to clarify the spatio-temporal remodeling changes caused by nerve transposition repair.

Acknowledgments: *We would like to thank Bin-Bin Nie (Institute of High Energy Physics, Chinese Academy of Sciences) and Gang Li (Institute of Materia Medica, Chinese Academy of Medical Sciences & Peking Union Medical College) for f-MRI data analysis assistance.*
Author contributions: *Study design, evaluation, and paper modification: PXZ; experimental implementation and data analysis manuscript writing: YSY, HLX, ZDL, YHK, BJ. manuscript writing: YSY, HLX. All authors approved the final version of the manuscript.*
Conflicts of interest: *The authors declare that they have no conflict of interest.*
Financial support: *This study was supported by the National Natural Science Foundation of China, Nos. 31771322, 81671215 (to PXZ); the Beijing National Science Foundation, Nos. 7212121 (to PXZ); the National Key Research and Development Plan of China, No. 2018YFB1105504 (to PXZ); Shenzhen Science and Technology Plan Project, No. JCYJ20190806162205278 (to PXZ); Sanming Project, No. SZSM202011001 (to PXZ); the Fundamental Research Funds for the Central Universities, Clinical Medicine Plus X - Young Scholars Project of Peking University China, No. PKU2020LCXQ020 (to YHK); the Key Laboratory of Trauma and Neural Regeneration (Peking University), the Ministry of Education China, No. BMU2019XY007-01; and the Ministry of Education Innovation Program of China, No. IRT_16R01. The funding sources had no role in study conception and design, data analysis or interpretation, paper writing or deciding to submit this paper for publication.*
Institutional review board statement: *The study was approved by the Ethics Committee of Peking University People's Hospital on December 9, 2015 (approval No. 2015-50).*

Data sharing statement: *Datasets analyzed during the current study are available from the corresponding author on reasonable request.*
Plagiarism check: *Checked twice by iThenticate.*
Peer review: *Externally peer reviewed.*

Open peer reviewers: *Maria Marcella Lagana, National Institute for Research and Treatment, Italy; Alberto Ballestin, Jesús Usón Minimally Invasive Surgery Center, Spain.*
Additional file: *Open peer review reports 1 and 2.*

References

Auer T, Pinter S, Kovacs N, Kalmar Z, Nagy F, Horvath RA, Koszo B, Kotek G, Perlaki G, Koves M, Kalman B, Komoly S, Schwarcz A, Woermann FG, Janszky J (2009) Does obstetric brachial plexus injury influence speech dominance? Ann Neurol 65:57-66.
Barkhof F, Haller S, Rombouts SA (2014) Resting-state functional MR imaging: a new window to the brain. Radiology 272:29-49.
Bhat DI, Indira Devi B, Bharti K, Panda R (2017) Cortical plasticity after brachial plexus injury and repair: a resting-state functional MRI study. Neurosurg Focus 42:E14.
Chao-Gan Y, Yu-Feng Z (2010) DPARSF: A MATLAB toolbox for "Pipeline" data analysis of resting-state fMRI. Front Syst Neurosci 4:13.
Chen YL, Xu L, Xu SJ (2020) Effects of physical activity on hippocampal plasticity and cognition. Zhongguo Zuzhi Gongcheng Yanjiu 24:773-779.
Ciumas C, Montavont A, Ryvlin P (2008) Magnetic resonance imaging in clinical trials. Curr Opin Neurol 21:431-436.
Costa RM, Cohen D, Nicolelis MA (2004) Differential corticostriatal plasticity during fast and slow motor skill learning in mice. Curr Biol 14:1124-1134.
Dąbrowski J, Czajka A, Zielińska-Turek J, Jaroszyński J, Furtak-Niczyporuk M, Mela A, Poniatowski Ł A, Drop B, Dorobek M, Barcikowska-Kotowicz M, Ziemba A (2019) Brain functional reserve in the context of neuroplasticity after stroke. Neural Plast 2019:9708905.
Diedrichsen J, Kornysheva K (2015) Motor skill learning between selection and execution. Trends Cogn Sci 19:227-233.
Feng JT, Liu HQ, Hua XY, Gu YD, Xu JG, Xu WD (2016) Brain functional network abnormality extends beyond the sensorimotor network in brachial plexus injury patients. Brain Imaging Behav 10:1198-1205.
Fox MD, Raichle ME (2007) Spontaneous fluctuations in brain activity observed with functional magnetic resonance imaging. Nat Rev Neurosci 8:700-711.
Gao W, Lin W (2012) Frontal parietal control network regulates the anti-correlated default and dorsal attention networks. Hum Brain Mapp 33:192-202.
Gorrostieta C, Ombao H, Bédard P, Sanes JN (2012) Investigating brain connectivity using mixed effects vector autoregressive models. Neuroimage 59:3347-3355.
Kawabata H, Shibata T, Matsui Y, Yasui N (2001) Use of intercostal nerves for neurotization of the musculocutaneous nerve in infants with birth-related brachial plexus palsy. J Neurosurg 94:386-391.
Kotani T, Toshima Y, Matsuda H, Suzuki T, Ishizaki Y (1971) Postoperative results of nerve transposition in brachial plexus injury. Seikei Geka 22:963-966.
Lam Van Ba O, Barbe MF, Caremel R, Aharony S, Loutochin O, Jacques L, Wood MW, Tiwari E, Tuite GF, Campeau L, Corcos J, Ruggieri MR, Sr. (2018) Lumbar to sacral root rerouting to restore bladder function in a feline spinal cord injury model: Urodynamic and retrograde nerve tracing results from a pilot study. Neurourol Urodyn 37:153-162.
Li B, Chen L, Gu YD (2020a) Stability of motor endplates is greater in the biceps than in the interossei in a rat model of obstetric brachial plexus palsy. Neural Regen Res 15:1678-1685.
Li NY, Onor GI, Lemme NJ, Gil JA (2020b) Epidemiology of peripheral nerve injuries in sports, exercise, and recreation in the United States, 2009-2018. Phys Sportsmed doi: 10.1080/00913847.2020.1850151.
Liang S, Wu S, Huang Q, Duan S, Liu H, Li Y, Zhao S, Nie B, Shan B (2017) Rat brain digital stereotaxic white matter atlas with fine tract delineation in Paxinos space and its automated applications in DTI data analysis. Magn Reson Imaging 43:122-128.
Liu B, Li T, Tang WJ, Zhang JH, Sun HP, Xu WD, Liu HQ, Feng XY (2013) Changes of inter-hemispheric functional connectivity between motor cortices after brachial plexuses injury: a resting-state fMRI study. Neuroscience 243:33-39.
Lu Y, Liu H, Hua X, Xu WD, Xu JG, Gu YD (2016) Supplementary motor cortical changes explored by resting-state functional connectivity in brachial plexus injury. World Neurosurg 88:300-305.
Makin TR, Filippini N, Duff EP, Henderson Slater D, Tracey I, Johansen-Berg H (2015) Network-level reorganisation of functional connectivity following arm amputation. Neuroimage 114:217-225.
Markov NT, Ercsey-Ravasz M, Van Essen DC, Knoblauch K, Toroczkai Z, Kennedy H (2013) Cortical high-density counterstream architectures. Science 342:1238406.
Nie B, Liu H, Chen K, Jiang X, Shan B (2014) A statistical parametric mapping toolbox used for voxel-wise analysis of FDG-PET images of rat brain. PLoS One 9:e108295.
Nie B, Hui J, Wang L, Chai P, Gao J, Liu S, Zhang Z, Shan B, Zhao S (2010) Automatic method for tracing regions of interest in rat brain magnetic resonance imaging studies. J Magn Reson Imaging 32:830-835.
Nie B, Chen K, Zhao S, Liu J, Gu X, Yao Q, Hui J, Zhang Z, Teng G, Zhao C, Shan B (2013) A rat brain MRI template with digital stereotaxic atlas of fine anatomical delineations in paxinos space and its automated application in voxel-wise analysis. Hum Brain Mapp 34:1306-1318.
Tos P, Ronchi G, Papalia I, Sallen V, Legagneux J, Geuna S, Giacobini-Robecchi MG (2009) Chapter 4: Methods and protocols in peripheral nerve regeneration experimental research: part I-experimental models. Int Rev Neurobiol 87:47-79.
Xie Y, Schneider KJ, Ali SA, Hogikyan ND, Feldman EL, Brenner MJ (2020) Current landscape in motoneuron regeneration and reconstruction for motor cranial nerve injuries. Neural Regen Res 15:1639-1649.
Yang G, Chang KW, Chung KC (2015a) A systematic review of contralateral c7 transfer for the treatment of traumatic brachial plexus injury: Part 1. Overall outcomes. Plast Reconstr Surg 136:794-809.
Yang G, Chang KW, Chung KC (2015b) A systematic review of outcomes of contralateral c7 transfer for the treatment of traumatic brachial plexus injury: Part 2. Donor-site morbidity. Plast Reconstr Surg 136:480e-489e.
Yang H, Long XY, Yang Y, Yan H, Zhu CZ, Zhou XP, Zang YF, Gong QY (2007) Amplitude of low frequency fluctuation within visual areas revealed by resting-state functional MRI. Neuroimage 36:144-152.
Zang Y, Jiang T, Lu Y, He Y, Tian L (2004) Regional homogeneity approach to fMRI data analysis. Neuroimage 22:394-400.
Zhang ZG, Chopp M (2009) Neurorestorative therapies for stroke: underlying mechanisms and translation to the clinic. Lancet Neurol 8:491-500.
Zheng MX, Hua XY, Feng JT, Li T, Lu YC, Shen YD, Cao XH, Zhao NQ, Lyu JY, Xu JG, Gu YD, Xu WD (2018) Trial of contralateral seventh cervical nerve transfer for spastic arm paralysis. N Engl J Med 378:22-34.
Zou QH, Zhu CZ, Yang Y, Zuo XN, Long XY, Cao QJ, Wang YF, Zang YF (2008) An improved approach to detection of amplitude of low-frequency fluctuation (ALFF) for resting-state fMRI: fractional ALFF. J Neurosci Methods 172:137-141.

P-Reviewers: Lagana MM, Ballestin A; C-Editor: Zhao M; S-Editors: Yu J, Li CH; L-Editors: Patel B, Yu J, Song LP; T-Editor: Jia Y